Int. J. Adv. Appl. Math. and Mech. 10(2) (2022) 15 – 26 (ISSN: 2347-2529)

Journal homepage: www.ijaamm.com

IJAAMM

International Journal of Advances in Applied Mathematics and Mechanics

Numerical simulation of changes in Soret-Dufour number, Radiation, chemical reaction and viscous dissipation on unsteady MHD flow past an inclined porous plate embedded in porous medium with heat generation or absorption

Research Article

A.K. Shukla*, **Shubham Kumar Dube**

Department of Mathematics,RSKD PG College Jaunpur, UP, India-222001

Received 23 September 2022; accepted (in revised version) 13 October 2022

Abstract: This paper aims to investigate the combined effects of Soret-Dufour and radiation on the unsteady MHD flow of a viscous incompressible and electrically conducting fluid past an impulsively started porous plate embedded in porous medium along with viscous dissipation, chemical reaction, heat generation or absorption with variable temperature, and mass diffusion. For various values of the flow parameters, the governing equations are numerically solved using the Crank-Nicolson finite difference method. Graphs and tables are used to explain the velocity, temperature, concentration, skin friction, Nusselt number, and Sherwood number.

MSC: 76W05 • 76R50 • 78A40 • 76M20 • 80A32

Keywords: MHD, Soret effect • Dufour effect • thermal radiation • porous medium • Heat and mass transfer • chemical reaction • Crank-Nicolson finite difference method

1. Introduction

MHD convective flow issues are significant in the industrial region in the fields of planetary magnetospheres, aviation, chemical engineering, nuclear reactors, and geothermal energy. Pure fluid does not occur in nature; instead, it contains certain contaminants. The ignorance of chemical reactions is not justified if the reaction level is high, and soret-Dufour effects are important if density differences exist in the flow regime.

The impact of a magnetic field on free convective heat transfer was studied by Sparrow et al.[13] The impacts of changing characteristics, hall current, and stable MHD laminar convective fluid flow because of a porous rotating disc were explored by Sattar et al.[9]. In a vertical channel, Anand Rao et al.[7] explored the effects of an applied magnetic field on transient free convective flow of an incompressible viscous dissipative fluid. The influence of radiation on MHD free convective flow of a radiation gas past a semi-infinite vertical plate was discussed by Gorla et al. [6] in their study. In a porous media with variable permeability and a heat source or sink, MHD fluctuating free convective flow with embedded radiation was described by Agarwal et al.[1].

Reddy et al.[8] examined the Soret effect on a flow of unsteady MHD free convective mass transfer past an infinite vertical porous plate with oscillatory suction velocity and heat sink. The effects of Dufour and Soret numbers on an

* Corresponding author.
E-mail address(es): ashishshukla1987@gmail.com (A.K. Shukla).

unsteady MHD flow past an infinite vertical porous plate with thermal radiation were numerically examined by Laxmi Narayan Gari et al.[5]. Mat Noor NA et al.[11] investigated Soret and Dufour effects on MHD squeezing flow of Jeffrey fluid in horizontal channel with thermal radiation. B. Shilpa et al. [12] studied Soret and Dufour effects on MHD double-diffusive mixed convective heat and mass transfer of couple stress fluid in a channel formed by electrically conducting and non-conducting walls. Deka et al.[4] examined how a first-order chemical reaction affected the flow through an infinite, vertical plate that was initiated abruptly and had constant heat flux and mass transfer.

Siddique et al. [10] looked at the unsteady energy and mass transport of a second-grade MHD nanofluid over an exponentially extending surface with Dufour and Soret effects. Soret-Dufour effects on unsteady MHD mixed convection for a heat-generating fluid with thermal radiation and chemical reaction have drawn the attention of many mathematicians as a result of all these works. The primary goal of this study is to investigate the effects of radiation and Soret-Dufour on unsteady MHD flow across an inclined porous plate embedded in a porous medium with viscous dissipation, chemical reaction, and heat generation or absorption. The Crank-Nicolson implicit finite difference approach is used to numerically solve the flow's governing equations.

2. Mathematical Analysis

Consider an unsteady flow of a viscous incompressible electrically conducting fluid past an impulsively moving infinite inclined porous plate with variable temperature and mass diffusion with Soret-Dufour effect, radiation effect, viscous dissipation, chemical reaction and heat source or sink have been studied. x^*-axis is taken along plate and y^*-axis is normal to it. Plate is inclined at angle α to vertical and embedded in porous medium. Initially fluid and plate are at same temperature and concentration, T^*_∞ and C^*_∞ respectively. At time t^*, the plate moves impulsively along direction of x^*-axis with constant velocity u_0 against gravitational field. Temperature and concentration of plate raise exponentially with time t^*. A transverse magnetic field of uniform strength B_0 is considered normal to flow direction, it is very small in comparison of magnetic Reynolds number, so induced magnetic field is negligible, Cowling [3].

Because of infinite length in x^* direction, flow variables are function of y^* and t^* only. Considering idea of usual Boussinesq approximation, the governing equations of this flow problem are given by:
Continuity equation:

$$\frac{\partial v^*}{\partial y^*} = 0 \Rightarrow v^* = -v_0 (constant) \tag{1}$$

Momentum equation:

$$\frac{\partial u^*}{\partial t^*} + v^* \frac{\partial u^*}{\partial y^*} = \lambda \frac{\partial^2 u^*}{\partial y^{*2}} + g\gamma (T^* - T^*_\infty) cos(\alpha) + g\gamma^* (C^* - C^*_\infty) cos(\alpha) - \frac{\sigma B_0^2 u^*}{\rho} - \frac{\lambda u^*}{K^*} \tag{2}$$

Energy equation:

$$\rho C_p \left(\frac{\partial T^*}{\partial t^*} + v^* \frac{\partial T^*}{\partial y^*} \right) = k \frac{\partial^2 T^*}{\partial y^{*2}} - \frac{\partial q_r}{\partial y^*} + \frac{\rho D_m K_T}{c_s} \frac{\partial^2 C^*}{\partial y^{*2}} + \mu \left(\frac{\partial u^*}{\partial y^*} \right)^2 - Q_0 (T^* - T^*_\infty) \tag{3}$$

Equation of continuity for mass transfer:

$$\frac{\partial C^*}{\partial t^*} + v^* \frac{\partial C^*}{\partial y^*} = D \frac{\partial^2 C^*}{\partial y^{*2}} + \frac{D_m K_T}{T_m} \frac{\partial^2 T^*}{\partial y^{*2}} - K_r (C^* - C^*_\infty) \tag{4}$$

where u^* and v^* are the velocity component along x^* and y^* directions respectively. γ^* is the coefficient of volume expansion for mass transfer, γ is the volumetric coefficient of thermal expansion, g is the acceleration due to gravity, λ is the kinematic viscosity, μ is viscosity, ρ is the fluid density, B_0 is magnetic induction, K^* is the permeability of porous medium, σ is the electrical conductivity of the fluid, T^* is the dimensional temperature, T^*_∞ is temperature of free stream, C^*_∞ is concentration of free stream, D_m is the chemical molecular diffusivity, k is the thermal conductivity of the fluid , K_r is chemical reaction parameter, the term $Q_0(T^* - T^*_\infty)$ is considered to be amount of heat generated or absorbed per unit volume where Q_0 is constant(for heat source $Q_0 > 0$ and for heat sink $Q_0 < 0$), c_p is specific heat at constant pressure, K_T is thermal diffusion ratio, C^* is the dimensional concentration, q_r is radiative heat flux in y^*-direction and T_m is mean fluid temperature.

Boundary and initial conditions are as follows:

$$\begin{aligned} t^* \le 0 \quad u^* = 0 \quad T^* = T^*_\infty \quad C^* = C^*_\infty \quad \forall y^* \\ t^* > 0 \quad u^* = u_0 \quad v^* = -v_0 \quad T^* = T^* + (T^*_w - T^*_\infty) e^{At^*}, \\ C^* = C^* + (C^*_w - C^*_\infty) e^{At^*} \quad at\ y^* = 0 \\ u^* = 0 \quad T^* \to \infty \quad C^* \to \infty \quad y^* \to \infty \end{aligned} \tag{5}$$

where, $A = \frac{v_0^2}{\lambda}$, T_w^* and C_w^* are tmeperature and concentration of plate respectively. The radiative heat flux term by using the Roseland approximation is given by

$$q_r = -\frac{4\sigma}{3k_l}\frac{\partial T^{*^4}}{\partial y^*} \tag{6}$$

where σ and k_l are Stefan Boltzmann constant and mean absorption coefficient respectively. It is supposed that the temperature difference within the flow is sufficiently small such that T^{*^4} may be expressed as a linear function of the temperature. It is done by expanding in a Taylor series about T_∞^* and neglecting the higher order terms, thus

$$T^{*^4} \cong 4T_\infty^{*^3}T^* - 3T_\infty^{*^4} \tag{7}$$

then using eq. (6) and eq. (7), equation eq. (3) is reduced as

$$\rho C_p\left(\frac{\partial T^*}{\partial t^*} + v^*\frac{\partial T^*}{\partial y^*}\right) = k\frac{\partial^2 T^*}{\partial y^{*^2}} + \frac{16\sigma T_\infty^{*^3}}{3k_l}\frac{\partial^2 T^*}{\partial y^{*^2}} + \frac{\rho D_m K_T}{c_s}\frac{\partial^2 C^*}{\partial y^{*^2}} + \mu\left(\frac{\partial u^*}{\partial y^*}\right)^2 - Q_0(T^* - T_\infty^*) \tag{8}$$

In order to obtain non-dimensional partial differential equations, introducing following dimensionless quantities:

$$\begin{gathered} u = \frac{u^*}{u_0},\ t = \frac{t^* v_0^2}{\lambda},\ \theta = \frac{T^* - T_\infty^*}{T_w^* - T_\infty^*},\ C = \frac{C^* - C_\infty^*}{C_w^* - C_\infty^*},\ Gm = \frac{\lambda g\alpha^*(C_w^* - C_\infty^*)}{u_0 v_0^2}, \\ Gr = \frac{\lambda g\alpha(T_w^* - T_\infty^*)}{u_0 v_0^2},\ Du = \frac{D_m K_T(C_w^* - C_\infty^*)}{c_s c_p \lambda(T_w^* - T_\infty^*)},\ Sr = \frac{D_m K_T(T_w^* - T_\infty^*)}{T_m\lambda(C_w^* - C_\infty^*)}, \\ K = \frac{v_0^2 K^*}{\lambda^2,},\ Pr = \frac{\mu c_p}{k},\ M = \frac{\sigma B_0^2\lambda}{\rho v_0^2},\ R = \frac{4\sigma T_\infty^{*^3}}{k_l k},\ k_r = \frac{K_r\lambda}{v_0^2},\ Q = \frac{Q_0\lambda}{\rho c_p v_0^2}, \\ Sc = \frac{\lambda}{D_m},\ Ec = \frac{u_0^2}{c_p(T_w^* - T_\infty^*)},\ y = \frac{y^* v_0}{\lambda} \end{gathered} \tag{9}$$

By virtue of eq. (9), we get non-dimensional form of eqs. (2), (3) and (8) respectively:

$$\frac{\partial u}{\partial t} - \frac{\partial u}{\partial y} = \frac{\partial^2 u}{\partial y^2} + Gr\cos(\alpha) + Gm\cos(\alpha) - \left(M + \frac{1}{K}\right)u \tag{10}$$

$$\frac{\partial \theta}{\partial t} - \frac{\partial \theta}{\partial y} = \frac{1}{Pr}\left(1 + \frac{4R}{3}\right)\frac{\partial^2\theta}{\partial y^2} + Du\frac{\partial^2 C}{\partial y^2} + Ec\left(\frac{\partial u}{\partial y}\right)^2 - Q\theta \tag{11}$$

$$\frac{\partial C}{\partial t} - \frac{\partial C}{\partial y} = \frac{1}{Sc}\frac{\partial^2 C}{\partial y^2} + Sr\frac{\partial^2\theta}{\partial y^2} - k_r C \tag{12}$$

with the following initial and boundary condition in non-dimensional quantities are:

$$\begin{array}{lllll} & t \le 0 & u = 0 & \theta = 0 & C = 0 \quad \forall y \\ t > 0 & u = 1 & \theta = e^t & C = e^t & at\ y = 0 \\ & u = 0 & u \to 0 & C \to 0 & y \to 0 \end{array} \tag{13}$$

Now it is of great importance to calculate the physical quantities local shear stress, local surface heat flux and Sherwood number for elementary interest.

Dimensionless local wall shear stress or skin-friction is acquired as,

$$\tau = \left(\frac{\partial u}{\partial y}\right)_{y=0} \tag{14}$$

Dimensionless local surface heat flux or Nusselt number is acquired as

$$Nu = -\left(\frac{\partial \theta}{\partial y}\right)_{y=0} \tag{15}$$

Dimensionless the local Sherwood number is obtained as

$$Sh = -\left(\frac{\partial C}{\partial y}\right)_{y=0} \tag{16}$$

3. Method of Solution

Equations (10) to (12) are coupled non-linear partial differential equations are solved using initial and boundary conditions (13). However exact solution of these equations is not possible, so we solve these equations using Crank-Nicolson implicit finite difference method for numerical solution. The equivalent finite difference scheme of eqs. (10) to (12) are given as:

$$\begin{aligned}\frac{u_{i,j+1}-u_{i,j}}{\Delta t}-\frac{u_{i+1,j}-u_{i,j}}{\Delta y}&=\left(\frac{u_{i-1,j}-2u_{i,j}+u_{i-1,j}-2u_{i,j+1}+u_{i+1,j+1}}{2(\Delta y)^2}\right)\\&+Gr\,cos(\alpha)\left(\frac{\theta_{i,j+1}-\theta_{i,j}}{2}\right)+Gm\,cos(\alpha)\left(\frac{Ci,j+1-Ci,j}{2}\right)\\&-\left(M+\frac{1}{K}\right)\left(\frac{u_{i,j+1}+u_{i,j}}{2}\right)\end{aligned}\tag{17}$$

$$\begin{aligned}\frac{\theta_{i,j+1}-\theta_{i,j}}{\Delta t}-\frac{\theta_{i+1,j}-\theta_{i,j}}{\Delta y}&=\frac{1}{Pr}\left(1+\frac{4R}{3}\right)\left(\frac{\theta_{i-1,j}-2\theta_{i,j}+\theta_{i-1,j}-2\theta_{i,j+1}+\theta_{i+1,j+1}}{2(\Delta y)^2}\right)\\&+Du\left(\frac{C_{i-1,j}-2u_{i,j}+C_{i-1,j}-2C_{i,j+1}+C_{i+1,j+1}}{2(\Delta y)^2}\right)\\&+Ec\left(\frac{u_{i+1,j}-u_{i,j}}{\Delta y}\right)^2-Q\left(\frac{\theta_{i,j+1}+\theta_{i,j}}{2}\right)\end{aligned}\tag{18}$$

$$\begin{aligned}\frac{C_{i,j+1}-C_{i,j}}{\Delta t}-\frac{C_{i+1,j}-C_{i,j}}{\Delta y}&=\frac{1}{Sc}\left(\frac{C_{i-1,j}-2u_{i,j}+C_{i-1,j}-2C_{i,j+1}+C_{i+1,j+1}}{2(\Delta y)^2}\right)\\&+Sr\left(\frac{\theta_{i-1,j}-2\theta_{i,j}+\theta_{i-1,j}-2\theta_{i,j+1}+\theta_{i+1,j+1}}{2(\Delta y)^2}\right)\\&-k_r\left(\frac{C_{i,j+1}+C_{i,j}}{2}\right)\end{aligned}\tag{19}$$

corresponding initial and boundary conditions are

$$\begin{aligned}u_{i,0}=0\quad\theta_{i,0}=0\quad C_{i,0}=0\quad\forall\, i\\u_{0,j}=1\quad\theta_{0,j}=e^{j\Delta t}\quad C_{0,j}=e^{j\Delta t}\\u_{X,j}=0\quad\theta_{X,j}\to 0\quad C_{X,j}\to 0\end{aligned}\tag{20}$$

Here j refers to time t, index i refers to y, $\Delta y=y_{i+1}-y_i$ and $\Delta t=t_{j+1}-t_j$. Getting the values of u, θ and C at time t, the values at time $t+\Delta t$ can be computed as follows: we substitute $i=1,2,3,....,X-1$ and X correspond to ∞, from eqs. (17) to (19) we achieve tridiagonal system of equations, can be figured out by Thomas algorithm as studied in Carnahan et al. [2]. Hereafter θ and C are known for all values of y at time $t+\Delta t$. Using values of θ and C in eq. (17) and computed by same procedure with initial and boundary condition, we get solution for u till desired time.

The implicit Crank-Nicolson finite difference method is a second order method $\left(o\left(\Delta t^2\right)\right)$ in time and has no restriction on space and time steps, that is, the method is unconditionally stable. The computation has been executed for $\Delta y=0.1, \Delta t=0.001$ and procedure is repeated till $y=4$.

4. Result and Discussion

Getting information from physical problem, numerical results for non-dimensional velocity field u, temperature field θ and concentration field C are demonstrated with the help of graphs by defining numerical values of thermal Grashof number Gr, the solutal Grashof number Gm, magnetic parameter M, prandtl number Pr, Schmidt number Sc, radiation parameter R, soret number Sr, chemical reaction parameter Kr, heat absorption or generation constant Q, inclination angle α and Eckert number Ec.

Figures 1 to 3 depict the variation of dimensionless velocity field u, temperature field θ and concentration field C respectively against the influence of physical parameter Sr. it is noted that on increasing soret number Sr, velocity field u increases rapidly near the plate, for same temperature field θ first decrease then increase while concentration field C increases. For different values of parameter Ec, it is seen that velocity profile increases in fig. 4, temperature profile also increases rapidly in fig. 5 and concentration profile first decreases after then increase in fig. 6 as parameter Ec increases. Figure 7 shows that velocity profile increases, fig. 8 displays that temperature profile increases rapidly and fig. 9 depict that concentration first increases then decrease when radiation parameter R increases. it is seen that velocity profile decreases in fig. 10, temperature profile in fig. 11 increases first after then decreases and concentration

profile in fig. 12 decreases as Schmidt number Sc increases. Velocity profile decreases in fig. 13, temperature profile decreases rapidly in fig. 14 and concentration profile first increases after then decreases in fig. 15 as prandtl number Pr increases.

It is noticed that velocity profile decreases in fig. 16, temperature profile increases slightly in fig. 17 and concentration profile decreases rapidly in fig. 18 when chemical reaction parameter K_r increases. Figure 19 depict that velocity profile increases slightly, in fig. 20 temperature profile rapidly increases and in fig. 21 concentration profile increases as Dufour number Du increases. It is observed that in fig. 22 velocity profile decreases rapidly and in fig. 23 temperature profile decreases slowly when magnetic parameter M increases. In fig. 24, it is seen that velocity profile increases rapidly and temperature profile increases slightly in fig. 25 as solutal Grashof number Gm increases. fig. 26 demonstrate that velocity profile increases rapidly as increases permeability of porous medium K and fig. 27 shows that velocity profile increases rapidly as inclination angle α increases. It is observed in fig. 28, velocity profile increases rapidly and in fig. 29 temperature profile increases slightly as thermal Grashof number Gr increases.

Velocity profile, temperature profile and concentration profile increases in figures 30, 31 and 32 respectively as time increases . In fig. 33 it is analyzed that velocity profile increases for heat sink and decreases for heat source, temperature profile decreases for heat source and increases for heat sink in fig. 34. It is also seen concentration profile increases for heat source and heat sink in fig. 35.

It is observed in table 1 that on increasing Dufour number Du, Eckert number Ec, solutal Grashof number Gm, thermal Grashof number Gr, permeability of porous medium K, radiation parameter R, Soret number Sr, coefficient of heat sink Q and time t skin friction coefficient increases while on increasing inclination angle α, chemical reaction parameter K_r, magnetic parameter M, prandtl number Pr, coefficient of heat source Q and Schmidt number Sc skin friction coefficient decreases.

Table 2 displays that Nusselt number Nu increases on increasing inclination angle α, Dufour number Du, permeability of porous medium K, magnetic parameter M, Prandtl number Pr, coefficient of heat source Q, Soret number Sr and time t on the contrary Nusselt number Nu decreases when Eckert number Ec, solutal Grashof number Gm, thermal Grashof number Gr, coefficient of heat sink Q, chemical reaction parameter K_r, radiation parameter R and Schmidt number Sc increase.

It is analyzed from table 3, Sherwood number increases as inclination angle α, Eckert number Ec, coefficient of heat sink Q, chemical reaction parameter K_r, radiation parameter R, Schmidt number Sc and time t increase on the other hand it decreases when Dufour number Du, solutal Grashof number Gm, thermal Grashof number Gr, permeability of porous medium K, magnetic parameter M, Prandtl number Pr, coefficient of heat source Q and Soret number Sr increase.

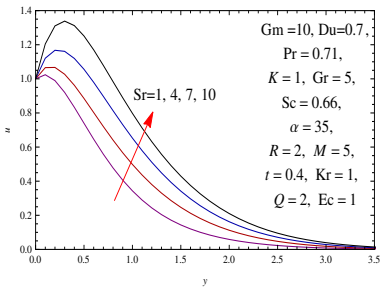

Fig. 1. Velocity Profile

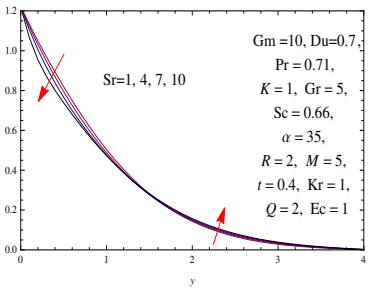

Fig. 2. Temperature Profile

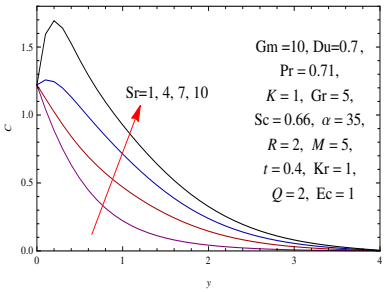

Fig. 3. Concentration Profile

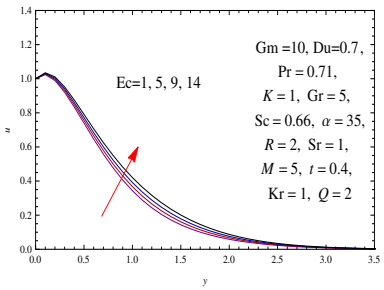

Fig. 4. Velocity Profile

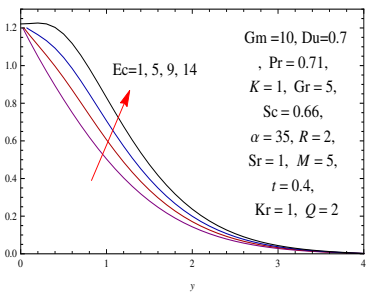

Fig. 5. Temperature Profile

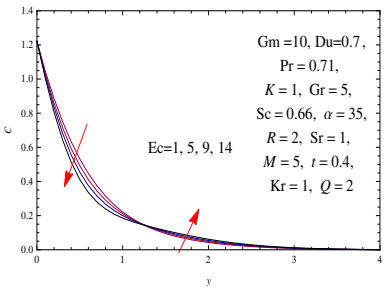

Fig. 6. Concentration Profile

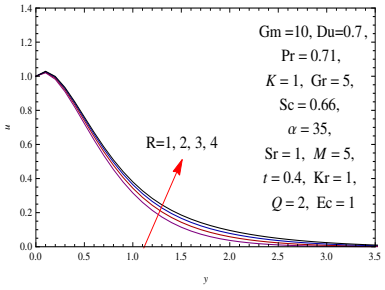

Fig. 7. Velocity Profile

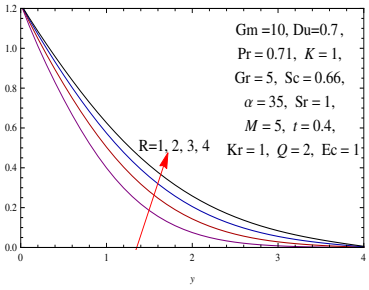

Fig. 8. Temperature Profile

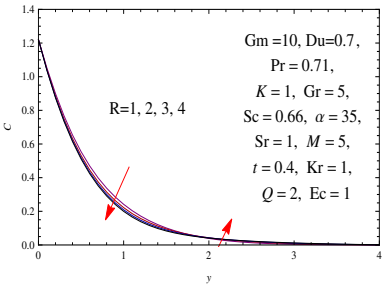

Fig. 9. Concentration Profile

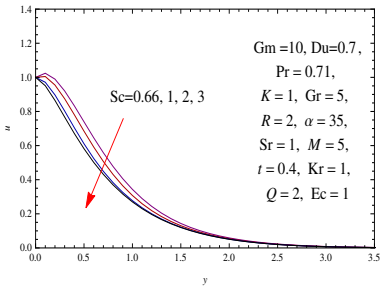

Fig. 10. Velocity Profile

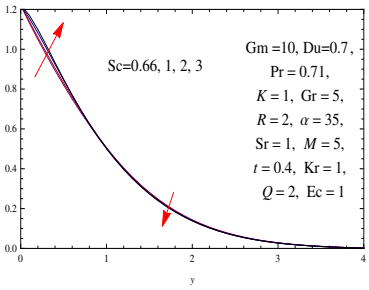

Fig. 11. Temperature Profile

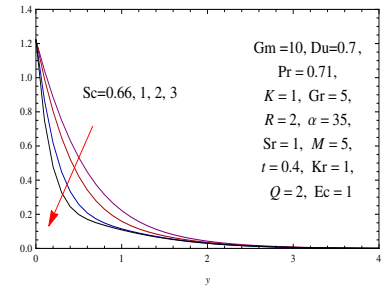

Fig. 12. Concentration Profile

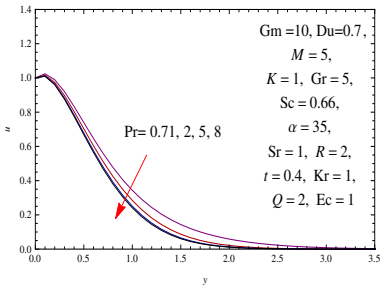

Fig. 13. Velocity Profile

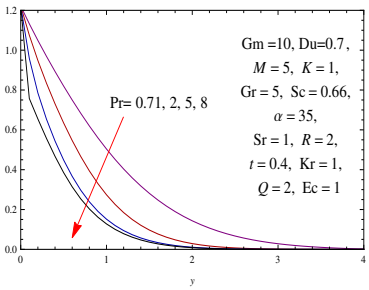

Fig. 14. Temperature Profile

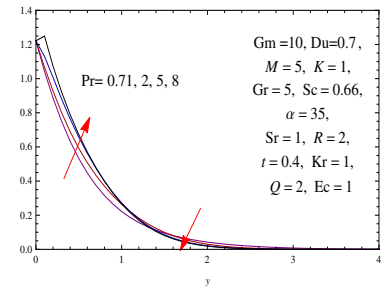

Fig. 15. Concentration Profile

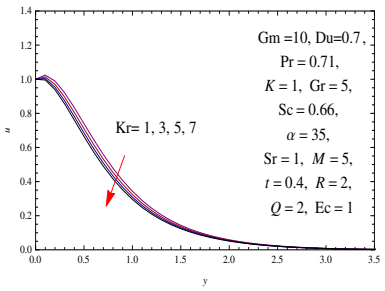

Fig. 16. Velocity Profile

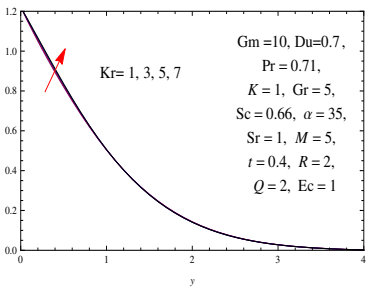

Fig. 17. Temperature Profile

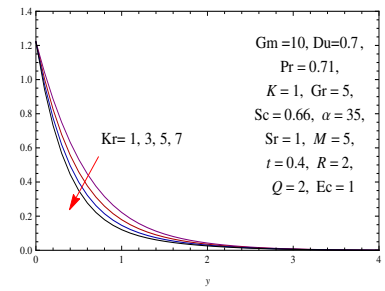

Fig. 18. Concentration Profile

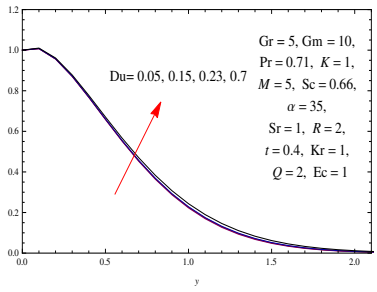

Fig. 19. Velocity Profile

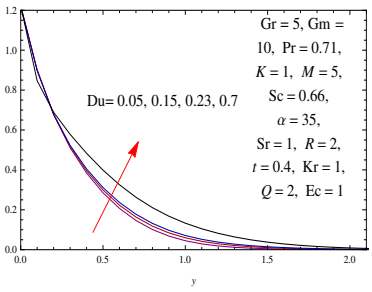

Fig. 20. Temperature Profile

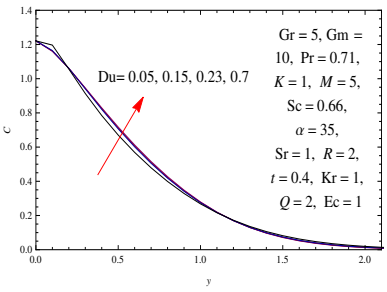

Fig. 21. Concentration Profile

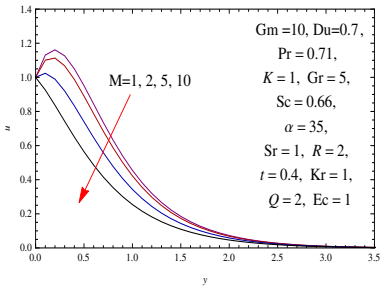

Fig. 22. Velocity Profile

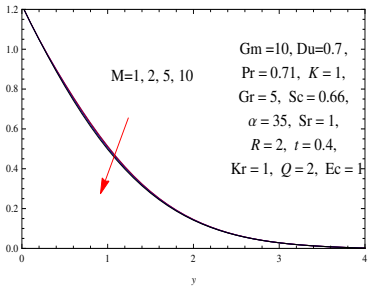

Fig. 23. Temperature Profile

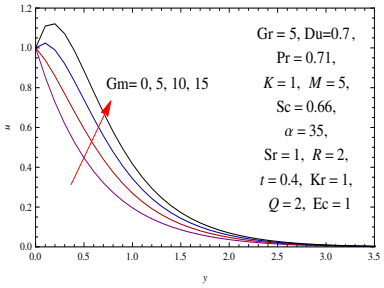

Fig. 24. Velocity Profile

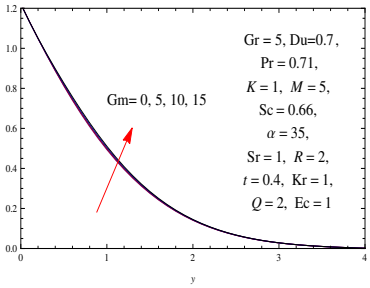

Fig. 25. Temperature Profile

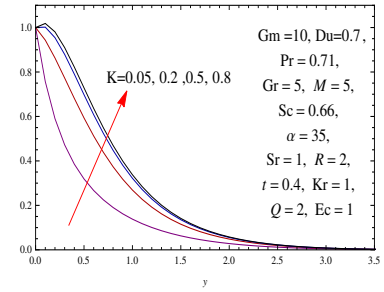

Fig. 26. Velocity Profile

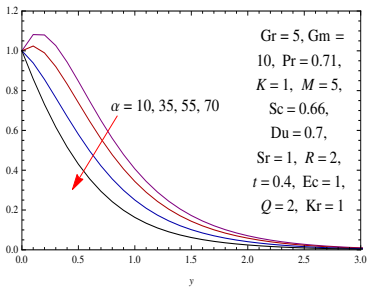

Fig. 27. Velocity Profile

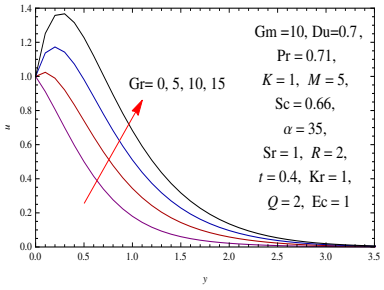

Fig. 28. Velocity Profile

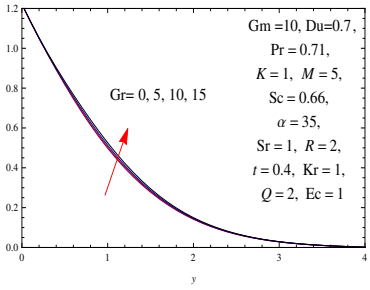

Fig. 29. Temperature Profile

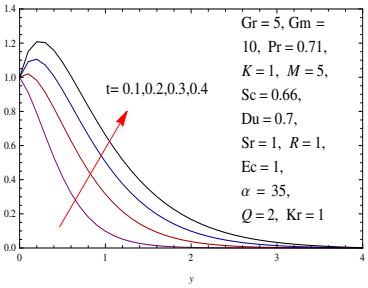

Fig. 30. Velocity Profile

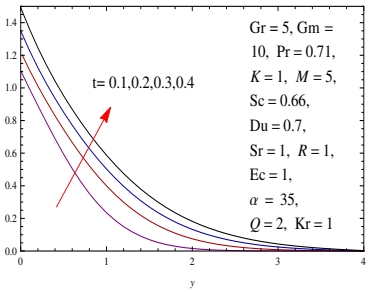

Fig. 31. Temperature Profile

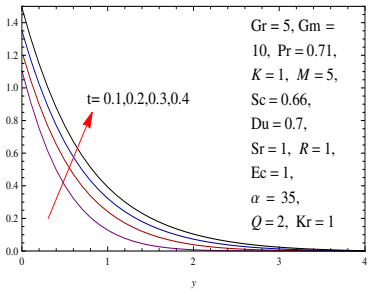

Fig. 32. Concentration Profile

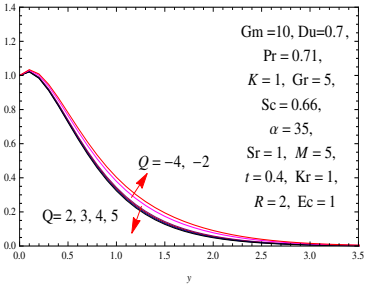

Fig. 33. Velocity Profile

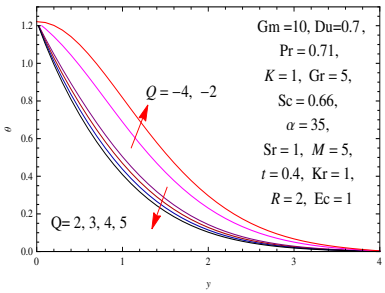

Fig. 34. Temperature Profile

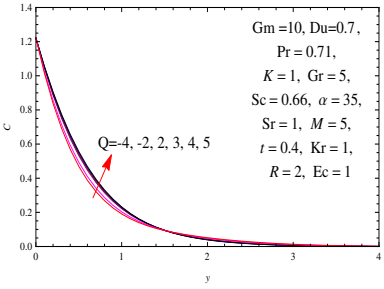

Fig. 35. Concentration Profile

Table 1. Skin friction coefficient for different values of parameters

Q	Kr	Du	Ec	K	M	Pr	R	Sc	Sr	Gm	Gr	γ	t	τ
−4	1	0.7	1	1	5	0.71	2	0.66	1	10	5	35	0.4	0.339231
−2	1	0.7	1	1	5	0.71	2	0.66	1	10	5	35	0.4	0.30039
3	1	0.7	1	1	5	0.71	2	0.66	1	10	5	35	0.4	0.229216
4	1	0.7	1	1	5	0.71	2	0.66	1	10	5	35	0.4	0.218289
5	1	0.7	1	1	5	0.71	2	0.66	1	10	5	35	0.4	0.208215
2	3	0.7	1	1	5	0.71	2	0.66	1	10	5	35	0.4	0.131988
2	5	0.7	1	1	5	0.71	2	0.66	1	10	5	35	0.4	0.0383531
2	7	0.7	1	1	5	0.71	2	0.66	1	10	5	35	0.4	−0.0426985
2	1	0.05	1	1	5	7	2	0.66	1	10	5	35	0.4	0.0716603
2	1	0.15	1	1	5	7	2	0.66	1	10	5	35	0.4	0.0760724
2	1	0.23	1	1	5	7	2	0.66	1	10	5	35	0.4	0.0796662
2	1	0.7	1	1	5	7	2	0.66	1	10	5	35	0.4	0.102485
2	1	0.7	5	1	5	0.71	2	0.66	1	10	5	35	0.4	0.27543
2	1	0.7	9	1	5	0.71	2	0.66	1	10	5	35	0.4	0.308353
2	1	0.7	14	1	5	0.71	2	0.66	1	10	5	35	0.4	0.34768
2	1	0.7	1	0.05	5	0.71	2	0.66	1	10	5	35	0.4	−2.43255
2	1	0.7	1	0.2	5	0.71	2	0.66	1	10	5	35	0.4	−0.56663
2	1	0.7	1	0.5	5	0.71	2	0.66	1	10	5	35	0.4	0.01912
2	1	0.7	1	0.8	5	0.71	2	0.66	1	10	5	35	0.4	0.18418
2	1	0.7	1	1	1	0.71	2	0.66	1	10	5	35	0.4	1.30613
2	1	0.7	1	1	2	0.71	2	0.66	1	10	5	35	0.4	1.00923
2	1	0.7	1	1	10	0.71	2	0.66	1	10	5	35	0.4	−0.739236
2	1	0.7	1	1	5	2	2	0.66	1	10	5	35	0.4	0.160613
2	1	0.7	1	1	5	5	2	0.66	1	10	5	35	0.4	0.112167
2	1	0.7	1	1	5	8	2	0.66	1	10	5	35	0.4	0.100765
2	1	0.7	1	1	5	0.71	1	0.66	1	10	5	35	0.4	0.203476
2	1	0.7	1	1	5	0.71	3	0.66	1	10	5	35	0.4	0.268306
2	1	0.7	1	1	5	0.71	4	0.66	1	10	5	35	0.4	0.289448
2	1	0.7	1	1	5	0.71	2	1	1	10	5	35	0.4	0.0489849
2	1	0.7	1	1	5	0.71	2	2	1	10	5	35	0.4	−0.287108
2	1	0.7	1	1	5	0.71	2	3	1	10	5	35	0.4	−0.489443
2	1	0.7	1	1	5	0.71	2	0.66	4	10	5	35	0.4	0.657274
2	1	0.7	1	1	5	0.71	2	0.66	7	10	5	35	0.4	1.21013
2	1	0.7	1	1	5	0.71	2	0.66	10	10	5	35	0.4	2.04687
2	1	0.7	1	1	5	0.71	2	0.66	1	0	5	35	0.4	−1.46998
2	1	0.7	1	1	5	0.71	2	0.66	1	5	5	35	0.4	−0.614758
2	1	0.7	1	1	5	0.71	2	0.66	1	15	5	35	0.4	1.09662
2	1	0.7	1	1	5	0.71	2	0.66	1	10	0	35	0.4	−0.889954
2	1	0.7	1	1	5	0.71	2	0.66	1	10	10	35	0.4	1.37512
2	1	0.7	1	1	5	0.71	2	0.66	1	10	15	35	0.4	2.51957
2	1	0.7	1	1	5	0.71	2	0.66	1	10	5	10	0.4	0.816387
2	1	0.7	1	1	5	0.71	2	0.66	1	10	5	55	0.4	−0.610522
2	1	0.7	1	1	5	0.71	2	0.66	1	10	5	70	0.4	−1.41261
2	1	0.7	1	1	5	0.71	2	0.66	1	10	5	35	0.1	−0.886541
2	1	0.7	1	1	5	0.71	2	0.66	1	10	5	35	0.2	0.203476
2	1	0.7	1	1	5	0.71	2	0.66	1	10	5	35	0.3	0.911775

Table 2. Nusselt number for different values of parameters

Q	Kr	Du	Ec	K	M	Pr	R	Sc	Sr	Gm	Gr	α	t	Nu
−4	1	0.7	1	1	5	0.71	2	0.66	1	10	5	35	0.4	0.369203
−2	1	0.7	1	1	5	0.71	2	0.66	1	10	5	35	0.4	2.08233
3	1	0.7	1	1	5	0.71	2	0.66	1	10	5	35	0.4	0.997221
4	1	0.7	1	1	5	0.71	2	0.66	1	10	5	35	0.4	1.10006
5	1	0.7	1	1	5	0.71	2	0.66	1	10	5	35	0.4	1.19709
2	3	0.7	1	1	5	0.71	2	0.66	1	10	5	35	0.4	0.842469
2	5	0.7	1	1	5	0.71	2	0.66	1	10	5	35	0.4	0.802177
2	7	0.7	1	1	5	0.71	2	0.66	1	10	5	35	0.4	0.766165
2	1	0.05	1	1	5	7	2	0.66	1	10	5	35	0.4	3.18995
2	1	0.15	1	1	5	7	2	0.66	1	10	5	35	0.4	3.22022
2	1	0.23	1	1	5	7	2	0.66	1	10	5	35	0.4	3.25114
2	1	0.7	1	1	5	7	2	0.66	1	10	5	35	0.4	3.7515
2	1	0.7	5	1	5	0.71	2	0.66	1	10	5	35	0.4	0.579347
2	1	0.7	9	1	5	0.71	2	0.66	1	10	5	35	0.4	0.297882
2	1	0.7	14	1	5	0.71	2	0.66	1	10	5	35	0.4	−0.019556
2	1	0.7	1	0.05	5	0.71	2	0.66	1	10	5	35	0.4	0.860185
2	1	0.7	1	0.2	5	0.71	2	0.66	1	10	5	35	0.4	0.884374
2	1	0.7	1	0.5	5	0.71	2	0.66	1	10	5	35	0.4	0.887714
2	1	0.7	1	0.8	5	0.71	2	0.66	1	10	5	35	0.4	0.88793
2	1	0.7	1	1	1	0.71	2	0.66	1	10	5	35	0.4	0.878584
2	1	0.7	1	1	2	0.71	2	0.66	1	10	5	35	0.4	0.88308
2	1	0.7	1	1	10	0.71	2	0.66	1	10	5	35	0.4	0.882748
2	1	0.7	1	1	5	2	2	0.66	1	10	5	35	0.4	1.46047
2	1	0.7	1	1	5	5	2	0.66	1	10	5	35	0.4	2.62685
2	1	0.7	1	1	5	8	2	0.66	1	10	5	35	0.4	4.63902
2	1	0.7	1	1	5	0.71	1	0.66	1	10	5	35	0.4	1.09469
2	1	0.7	1	1	5	0.71	3	0.66	1	10	5	35	0.4	0.771304
2	1	0.7	1	1	5	0.71	4	0.66	1	10	5	35	0.4	0.693257
2	1	0.7	1	1	5	0.71	2	1	1	10	5	35	0.4	0.823723
2	1	0.7	1	1	5	0.71	2	2	1	10	5	35	0.4	0.660832
2	1	0.7	1	1	5	0.71	2	3	1	10	5	35	0.4	0.510389
2	1	0.7	1	1	5	0.71	2	0.66	4	10	5	35	0.4	0.991854
2	1	0.7	1	1	5	0.71	2	0.66	7	10	5	35	0.4	1.15429
2	1	0.7	1	1	5	0.71	2	0.66	10	10	5	35	0.4	1.5533
2	1	0.7	1	1	5	0.71	2	0.66	1	0	5	35	0.4	0.872076
2	1	0.7	1	1	5	0.71	2	0.66	1	5	5	35	0.4	0.885352
2	1	0.7	1	1	5	0.71	2	0.66	1	15	5	35	0.4	0.879828
2	1	0.7	1	1	5	0.71	2	0.66	1	10	0	35	0.4	0.8656
2	1	0.7	1	1	5	0.71	2	0.66	1	10	10	35	0.4	0.885285
2	1	0.7	1	1	5	0.71	2	0.66	1	10	15	35	0.4	0.857014
2	1	0.7	1	1	5	0.71	2	0.66	1	10	5	10	0.4	0.886134
2	1	0.7	1	1	5	0.71	2	0.66	1	10	5	55	0.4	0.880767
2	1	0.7	1	1	5	0.71	2	0.66	1	10	5	70	0.4	0.863321
2	1	0.7	1	1	5	0.71	2	0.66	1	10	5	35	0.1	1.08326
2	1	0.7	1	1	5	0.71	2	0.66	1	10	5	35	0.2	1.09469
2	1	0.7	1	1	5	0.71	2	0.66	1	10	5	35	0.3	1.17925

Table 3. Sherwood number for different values of parameters

Q	Kr	Du	Ec	K	M	Pr	R	Sc	Sr	Gm	Gr	α	t	Sh
−4	1	0.7	1	1	5	0.71	2	0.66	1	10	5	35	0.4	1.97532
−2	1	0.7	1	1	5	0.71	2	0.66	1	10	5	35	0.4	2.08233
3	1	0.7	1	1	5	0.71	2	0.66	1	10	5	35	0.4	1.74466
4	1	0.7	1	1	5	0.71	2	0.66	1	10	5	35	0.4	1.70362
5	1	0.7	1	1	5	0.71	2	0.66	1	10	5	35	0.4	1.664
2	3	0.7	1	1	5	0.71	2	0.66	1	10	5	35	0.4	2.16313
2	5	0.7	1	1	5	0.71	2	0.66	1	10	5	35	0.4	2.48927
2	7	0.7	1	1	5	0.71	2	0.66	1	10	5	35	0.4	2.77575
2	1	0.05	1	1	5	7	2	0.66	1	10	5	35	0.4	0.6145
2	1	0.15	1	1	5	7	2	0.66	1	10	5	35	0.4	0.592351
2	1	0.23	1	1	5	7	2	0.66	1	10	5	35	0.4	0.570547
2	1	0.7	1	1	5	7	2	0.66	1	10	5	35	0.4	0.24922
2	1	0.7	5	1	5	0.71	2	0.66	1	10	5	35	0.4	1.93353
2	1	0.7	9	1	5	0.71	2	0.66	1	10	5	35	0.4	2.06729
2	1	0.7	14	1	5	0.71	2	0.66	1	10	5	35	0.4	2.21848
2	1	0.7	1	0.05	5	0.71	2	0.66	1	10	5	35	0.4	1.81015
2	1	0.7	1	0.2	5	0.71	2	0.66	1	10	5	35	0.4	1.79231
2	1	0.7	1	0.5	5	0.71	2	0.66	1	10	5	35	0.4	1.7883
2	1	0.7	1	0.8	5	0.71	2	0.66	1	10	5	35	0.4	1.78747
2	1	0.7	1	1	1	0.71	2	0.66	1	10	5	35	0.4	1.78651
2	1	0.7	1	1	2	0.71	2	0.66	1	10	5	35	0.4	1.7859
2	1	0.7	1	1	10	0.71	2	0.66	1	10	5	35	0.4	1.79376
2	1	0.7	1	1	5	2	2	0.66	1	10	5	35	0.4	1.53446
2	1	0.7	1	1	5	5	2	0.66	1	10	5	35	0.4	0.905749
2	1	0.7	1	1	5	8	2	0.66	1	10	5	35	0.4	−0.281407
2	1	0.7	1	1	5	0.71	1	0.66	1	10	5	35	0.4	1.70334
2	1	0.7	1	1	5	0.71	3	0.66	1	10	5	35	0.4	1.82969
2	1	0.7	1	1	5	0.71	4	0.66	1	10	5	35	0.4	1.85587
2	1	0.7	1	1	5	0.71	2	1	1	10	5	35	0.4	2.28276
2	1	0.7	1	1	5	0.71	2	2	1	10	5	35	0.4	3.54714
2	1	0.7	1	1	5	0.71	2	3	1	10	5	35	0.4	4.71357
2	1	0.7	1	1	5	0.71	2	0.66	4	10	5	35	0.4	0.996814
2	1	0.7	1	1	5	0.71	2	0.66	7	10	5	35	0.4	−0.367638
2	1	0.7	1	1	5	0.71	2	0.66	10	10	5	35	0.4	−3.72837
2	1	0.7	1	1	5	0.71	2	0.66	1	0	5	35	0.4	1.80217
2	1	0.7	1	1	5	0.71	2	0.66	1	5	5	35	0.4	1.79225
2	1	0.7	1	1	5	0.71	2	0.66	1	15	5	35	0.4	1.7871
2	1	0.7	1	1	5	0.71	2	0.66	1	10	0	35	0.4	1.80305
2	1	0.7	1	1	5	0.71	2	0.66	1	10	10	35	0.4	1.78317
2	1	0.7	1	1	5	0.71	2	0.66	1	10	15	35	0.4	1.79119
2	1	0.7	1	1	5	0.71	2	0.66	1	10	5	10	0.4	1.78541
2	1	0.7	1	1	5	0.71	2	0.66	1	10	5	55	0.4	1.79448
2	1	0.7	1	1	5	0.71	2	0.66	1	10	5	70	0.4	1.8063
2	1	0.7	1	1	5	0.71	2	0.66	1	10	5	35	0.1	1.68766
2	1	0.7	1	1	5	0.71	2	0.66	1	10	5	35	0.2	1.70334
2	1	0.7	1	1	5	0.71	2	0.66	1	10	5	35	0.3	1.72461

References

[1] Agarwal, M., Sharma, B. and Chaudhary, R. Mhd fluctuating free convective flow with radiation embedded in porous medium having variable permeability and heat source/sink, International Journal of Heat and Mass Transfer 87(1)(2006).: 47–58.

[2] Carnahan, H., Luthor, J. and Wilkes . Applied Numerical Methods, John Wiley and Sons, NewYork. (1969)

[3] Cowling, T. . Magnetohydro Dynamics, InterScience Publishers, NewYork (1957).

[4] Deka, R., Soundalgekar, V. and Das, U. . Effects of mass trasnfer on flow past an impulsively started infinite vertical plate with constant heat flux and chemical reaction, Forschung im Ingenieurwesen 60(10)(1994): 284–287.

[5] Gari, A. L. N. and Vempati, S. . Soret and dufour effects on unsteady mhd flow past an infinite vertical porous plate with thermal radiation, Applied Math and Mech. Eng. Ed. 13(12)(2010): 1481–1496.

[6] Goral, R., Takhar, H. and Soundlatgekar, V. . Radiation effects on mhd free convection flow of a radiation gas past a semi infinite vertical plate, International Journal of Numerical Method Heat fluid Flow 6 (1997): 7–38.

[7] Rao, J. A. and Raju, R. S. . Applied magnetic field on transient free convective flow of an incompressible viscous dissipation fluid in a vertical channel, Journal of Energy 32 (2010): 265– 277.

[8] Reddy, S., Hari, K. S. and Rao, J. . Soret effect on unsteady mhd free convective mass transfer flow past an infinite vertical porous plate with oscillatory suction velocity and heat sink, International Journal of Applied Mathematical Analysis and Application 1(2)(2006): 239– 259.

[9] Sattar, M. A. and Malique, K. A. . The effects of variable properties and hall current and steady mhd laminar convective fluid flow due to a porous rotating disk, International Journal of Heat and Mass Transfer 48 (2005): 4460–4466.

[10] Siddique, I., Nadeem, M., Awrejcewicz, J. et al. Soret and Dufour effects on unsteady MHD second-grade nanofluid flow across an exponentially stretching surface. Sci Rep 12, 11811 (2022). https://doi.org/10.1038/s41598-022-16173-8

[11] Mat Noor NA, Shafie S, Hamed YS, Admon MA. Soret and Dufour effects on MHD squeezing flow of Jeffrey fluid in horizontal channel with thermal radiation. PLoS One. 2022 May 19;17(5):e0266494. doi: 10.1371/journal.pone.0266494. PMID: 35587920; PMCID: PMC9126172.

[12] B. Shilpa, V. Leela, B. C. Prasannakumara & Pulla Nagabhushana (2022) Soret and Dufour effects on MHD double-diffusive mixed convective heat and mass transfer of couple stress fluid in a channel formed by electrically conducting and non-conducting walls, Waves in Random and Complex Media, DOI: 10.1080/17455030.2022.2119491

[13] Sparrow, E. and Cess, R. . Effect of magnetic field on free convection heat transfer, International Journal of Heat and Mass Transfer 3 (1961): 267–270.